CHEMISTRY AND PHYSICAL PROPERTIES OF AXINITES

by

Gregory Randolph Lumpkin

Thesis submitted to the Graduate Faculty of the
Virginia Polytechnic Institute and State University
in partial fulfillment of the requirements for the degree of

MASTER OF SCIENCE

in

Geological Sciences

APPROVED:

P.H. Ribbe, Chairman

G.V. Gibbs D.A. Hewitt

June, 1978

Blacksburg, Virginia

ACKNOWLEDGEMENTS

The writer would like to thank his major advisor,
, for encouragement and advice throughout the course of this research. The other members of the writer's committee,
and offered constructive criticisms of the thesis under adverse conditions. Specimens used in this study were provided by the National Museum of Natural History, the Academy of Natural Sciences of Philadelphia,
ran the calculated powder patterns at the U.S. Geological Survey in Reston, Virginia. Finally, the writer would like to express his appreciation to his wife, , and parents,
for their encouragement and support of this work.

TABLE OF CONTENTS

LIST OF TABLES

LIST OF FIGURES

INTRODUCTION

The axinite group of borosilicates, $[(Mn,Fe^{2+},Mg,Zn)(Ca,Mn)_2(Al,Fe^{3+})_2]_2(OH)_2[B_2Si_8O_{30}]$, are known from localities worldwide, occurring in skarns, ore deposits, pegmatites, and low-grade regional metamorphic rocks. Many authors have studied axinite and, although much information dealing with the chemical composition, density, and optical properties is available in the literature, many chemical analyses are of questionable accuracy, and no serious attempt has been made to relate the chemical and physical properties for the group as a whole. Few determinations of lattice parameters have been reported and their variation with composition has not been examined.

With the aid of multiple linear regression analysis, this study is designed to examine the relationships between chemical composition and (1) lattice parameters, (2) density, (3) refractive indices, and (4) 2V for the range of naturally occurring axinites, as represented by 37 specimens from 31 localities (see Table 1).

Table I. Localities and sources of axinites used in this study

Number	Locality	Source	Number	Locality	Source
1	Tinzens, Switzerland	NMNH[1] 95431	20	Thomaston, Connecticut	C. A. Francis
2	Obira, Japan	NMNH 15210	21	Plumas Co., California	J. B. Higgins
3	Cornwall, England	NMNH C 6011	22	Miyazaki, Japan	J. B. Higgins
4	Bourg d' Oisans, France	NMNH B 17121	23	Mineral Co., Nevada	J. A. Speer
5	Genova, Italy	NMNH 127774	24	Saxony, Germany	ANSP[2] 3118
6	Luning, Nevada	NMNH 94407-4	25	Caylloma, Peru	ANSP 20356
7	Obira, Japan	NMNH R 12503	26	Dannemora, Sweden	ANSP 23951
8	Mitchell Co., N.C.	NMNH 120244	27	Cornwall, England	ANSP 20104
9	Dauphine, France	NMNH R 14648	28	Northampton Co., Pa.	ANSP 9282
10	Bonsall, California	NMNH 93648	29	Tremola, Italy	ANSP 3521
11	Franklin,New Jersey	NMNH C 6233-1	30	Perkiomenville, Pa.	ANSP 22210
12	Rosebery, Australia	NMNH B 16838	31	Franklin, New Jersey	NMNH R 3847
13	Knappenwand, Austria	NMNH B 17136	32	Franklin, New Jersey	NMNH C 3145
14	Mt. Scopi, Switzerland	NMNH 80224	33	Huachuca Mtns., Arizona	NMNH 102822
15	Avondale, Pennsylvania	NMNH 87232	34	Mt. Scopi, Switzerland	NMNH B 17125
16	Kongsberg, Norway	NMNH B 17112	35	Woodlake, California	TM[3] 9620
17	Pferdekopf, Germany	NMNH B 17110	36	Franklin, New Jersey	NMNH 94946
18	Cornog, Pennsylvania	J. A. Speer	37	St. Maria, Switzerland	NMNH B 17127
19	Shadwell, Virginia	G. R. Lumpkin			

1 Specimens designated NMNH were donated by John S. White of the National Museum of Natural History.

2 Specimens designated ANSP were donated by Robert G. Middleton of the Academy of Natural Sciences of Philadelphia.

3 Specimen TM 9620 was donated by J. J. Finney of the Colorado School of Mines.

PREVIOUS STUDIES

Chemistry and Nomenclature

Among the earliest chemical analyses of axinites are those by Genth (1891), Dana (1892), Hintze (1897), and Ford (1903). Several of these are obviously incorrect, but from the available data Schaller (1911) was able to recognize the substitutional relationship of Mn and Fe^{2+} and propose the end-members *ferroaxinite*, $Al_2BHCa_2FeSi_4O_{16}$, and *manganoaxinite*, $Al_2BHCa_2MnSi_4O_{16}$. Schaller presumed that the Ca content of axinite was constant.

Now known to be a member of the axinite group, *tinzenite* was originally described as a distinct species by Jakob (1923, 1926, 1933), who had failed to analyze for B_2O_3. The crystallographic and optical similarities of tinzenite and axinite were noted by Parker (1948) and Waldmann (1948), and their isomorphism was finally established by Milton *et al.* (1953) using bulk chemical analyses and X-ray diffraction data. Variability in Ca content of Mn-rich axinites was also noted by Milton *et al.*

Sanero and Gottardi (1968) plotted 17 chemical analyses of axinite on a triangular diagram with vertices 3Ca - 3Mn - 3(Fe+Mg). All compositions plotted on either of two lines:

$$2Ca \cdot 1(Fe+Mg) \leftrightarrow 2Ca \cdot 1Mn \quad \text{or}$$

$$2Ca \cdot 1Mn \leftrightarrow 1Ca \cdot 2Mn.$$

They proposed the following nomenclature:

(1) *Axinite* as the group name.

(2) *Ferroaxinite* for Ca > 1.5, Fe > Mn.

(3) *Manganaxinite* for Ca > 1.5, Mn > Fe.

(4) *Tinzenite* for Ca < 1.5, Mn > Fe.

Whether Mn is ordered or disordered in the Ca-sites of tinzenite was open to question, so Sanero and Gottardi (1968) proposed the general formula $H(Ca,Fe,Mn,Mg)_3Al_2BSi_4O_{16}$.

A fourth end-member called *magnesioaxinite* was described by Jobbins *et al.* (1975). The specimen examined by these authors has a composition approaching $HCa_2MgAl_2BSi_4O_{16}$ with no Fe and only 0.4 wt.% MnO.

In a study of axinites from Devonshire, England, Chaudry and Howie (1969) found a "reciprocal relationship" between Mg and Mn (but not Fe^{2+} and Mn). In some of their bulk chemical analyses they noted a deficiency of Si with an excess of Al + Ti + Fe^{3+} and they suggested that Al may substitute for Si in tetrahedral coordination. Astakhov *et al.* (1976) examined the ^{57}Fe Mössbauer spectra of an axinite, and found two doublets corresponding to the two oxidation states of iron. They calculated that 5% of the iron was Fe^{3+}, and they assumed that it substituted for Al^{3+} in the AlO_5OH octahedra.

Physical Properties

Schaller (1911) noted an increase in density of axinite with increasing Mn content. Chaudry and Howie (1969) could make no correlation between density and composition over the very limited range of their study, but did show a moderate correlation between refractive indices and (Fe^{3+} + Mn + Fe^{2+} + Ti). Gadeke (1938) found a linear variation of mean refractive index with composition for five axinites

ranging in composition from 0.33% to 12.86% MnO; however, Milton *et al.* (1953) noted that tinzenite did not fall on Gadeke's curve, possibly due to low CaO content. Barbour *et al.* (1957) suggest that there is no correlation between optic axial angle 2V and the composition of axinite.

Crystal Structure

Peacock (1937) determined the reduced triclinic $P\bar{1}$ cell for axinite, and his paper contains an excellent review of earlier crystallographic studies. He determined lattice parameters using rotation and Weissenberg X-ray techniques and compared them to morphological determinations.

Ito and Takéuchi (1952) first studied the structure of axinite, describing separate Si_4O_{12} rings and BO_3 groups; however, infrared spectra (Plyusina, 1961; Moenke, 1962) and optical absorption spectra (Eremenko, 1971) indicated that boron was in tetrahedral coordination, and Plyusina (1961) suggested that discrete Si_4O_{12} rings did not exist in the structure. Reinvestigation of the structure by Ito *et al.* (1969) and Takéuchi *et al.* (1974) showed the existence of unique $B_2Si_8O_{30}$ groups in which two boron tetrahedra share three corners each, linking together four Si_2O_7 groups. A nearly rectangular six-membered ring consisting of four silicon- and two boron-containing tetrahedra lies approximately parallel to $(\bar{1}21)$ (Takéuchi *et al.*, 1974) and forms the center of each $B_2Si_8O_{30}$ group (Fig. 1a). These $B_2Si_8O_{30}$ groups are nearly planar in character and are arranged in distinct tetrahedral layers, alternating with sheets of edge-sharing octahedra. The octahedral layers are composed of finite chains of six

Figure 1

Projections down the *a*-axis of the axinite structure. (a) Tetrahedral layer: the $B_2Si_8O_{30}$ group with {100} cleavage traces shown as dashed lines parallel to $[0\bar{1}1]$. (b) The octahedral layer: OH atoms (large dots) lie on the {100} cleavage traces parallel to $[0\bar{1}1]$. Figures modified from Takéuchi *et al.* (1974).

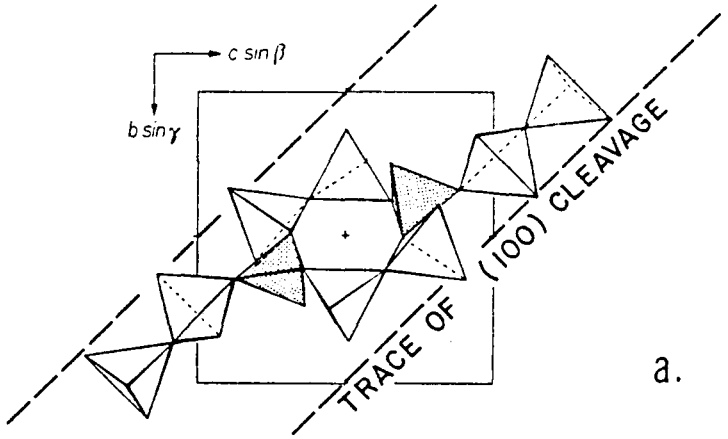
c sin β
b sin γ
TRACE OF (100) CLEAVAGE

a.

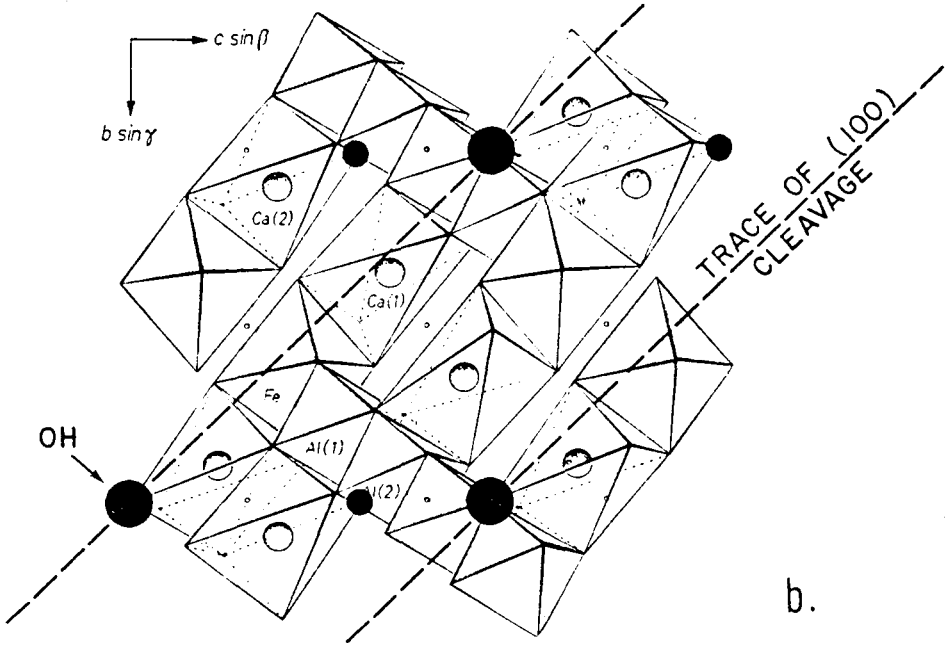
c sin β
b sin γ
Ca(2)
Ca(1)
Fe
Al(1)
Al(2)
OH
TRACE OF (100) CLEAVAGE

b.

octahedra of the type Fe-Al-Al-Al-Al-Fe, cross-linked by distorted CaO_6 and $CaO_5(OH)$ polyhedra (Fig. 1b).

EXPERIMENTAL PROCEDURES

Electron Microprobe Analysis

Hand-picked grains of axinite were mounted in epoxy, polished, and carbon-coated for analysis using a nine-spectrometer ARL-SEMQ microprobe operated at 15 kV, 100 nA. Elements analyzed for included Ti, Na and K (these three were not detected at the 0.05 wt.% level), Zn (found only in specimens from Franklin, New Jersey) and the major elements Ca, Fe, Mg, Mn, Al, B, and Si. A chemically analyzed axinite Bourg d'Oisans, France, 6.12 wt.% B_2O_3) was used as a boron standard, but count rates were extremely low (6-7 cps above background). For that reason boron was ultimately assumed to be stoichiometric, as was OH. Data reduction was accomplished using the program MAGIC IV by John Colby, adapted for the ARL-SEMQ by William Hamilton.

Density

Specimens weighing between 15 and 25 mg were hand-picked under a microscope for density measurements using a Berman balance with toluene as the buoyant medium (Berman, 1939). Each density reported is the mean of five determinations, each corrected for temperature.

Lattice Parameters

Lattice parameters of 10 axinites were determined using X-ray powder patterns with BaF_2 as an internal standard. The BaF_2 (a = 6.198(2) Å) was annealed five times for two hours each at 800°C (J.A. Speer, pers. comm.). The powder patterns were run on a Picker diffractometer with monochromatized Cu$K\alpha$ radiation, 1 inch/min. chart speed, 0.5° 2θ/min. scan rate, and a 1° receiving slit. Ambiguity in

indexing was overcome by reference to calculated powder patterns for each of the four axinite end-members based on the structure refinement of Takéuchi *et al.* (1974). These were kindly run by Judith Konnert of the U.S. Geological Survey, Reston, Virginia. The least-squares program of Appleman and Evans (1973) was used to refine the lattice parameters with starting parameters taken from Takéuchi *et al.* (1974).

Optical Properties

Refractive indices and the optic axial angle 2V were determined by the spindle stage technique of Bloss (in press). Using the computer program of Bloss and Riess (1973), optic axial angle and spindle stage coordinates for the measurement of refractive indices were calculated from extinction data taken in sodium light. For each principle vibration direction the wavelength of match was recorded in at least five refractive index oils. The index of match was then corrected for temperature, and the data were fitted to a linearized Sellmeier equation from which the refractive indices were calculated for sodium light. The maximum estimated error for refractive indices is ±0.001. The orientation of the biaxial indicatrix relative to the crystallographic directions (Fig. 4) was obtained for a manganaxinite from Franklin, N.J. (sample no. 11) by alignment of the crystal on an X-ray precession camera subsequent to its characterization on the spindle stage.

Chemical analyses, lattice parameters, densities, refractive indices, and 2V are compiled in Tables 2 and 3.

Table II

Microprobe analyses, refractive indices, 2Vα, density, and lattice parameters for 14 axinites.

Specimen	1	5	6	7	8	11	12	15	17	19	33	(35)	(1)	(3)
CaO (wt %)	12.01	13.77	20.15	19.00	19.71	18.59	19.18	19.27	20.12	19.71	18.76	19.59	*21.7*	*20.1*
MnO	20.74	18.57	3.35	5.83	9.48	12.36	2.61	9.55	1.23	3.23	12.39	6.59	*0.9*	*3.5*
FeO	2.48	0.55	4.32	6.44	2.85	1.88	10.41	3.41	7.94	7.83	1.10	5.21	*n.d.*	*6.1*
MgO	0.20	0.17	3.03	0.76	0.40	0.13	0.66	0.21	2.20	1.20	0.53	0.62	*6.9*	*1.6*
ZnO	n.d.	n.d.	n.d.	n.d.	n.d.	1.43	n.d.	n.d.	n.d.	n.d.	n.d.	n.d.	*0.06*	*n.d.*
Al_2O_3	15.41	17.95	18.52	18.63	17.27	16.61	17.24	17.80	18.21	17.96	17.45	17.83	*17.9*	*17.5*
$(B_2O_3)^A$	(6.00)	(6.04)	(6.26)	(6.14)	(6.11)	(6.10)	(6.14)	(6.12)	(6.21)	(6.16)	(6.12)	(6.13)	--	--
SiO_2	41.22	41.41	42.72	41.09	41.55	41.44	41.97	42.59	42.80	42.55	41.80	41.86	*41.0*	*42.2*
$(H_2O)^A$	(1.53)	(1.56)	(1.61)	(1.57)	(1.56)	(1.56)	(1.57)	(1.59)	(1.61)	(1.59)	(1.57)	(1.57)	--	--
Sum	99.59	100.02	99.96	99.46	98.93	100.10	99.78	100.54	100.32	100.23	99.72	99.40	--	--
Fe^{**}	0.655	0.578	0.249	0.383		0.456	0.396	0.400	0.291	0.346	0.412		*0.021*	
α	1.694	1.691	1.669	1.683		1.685	1.682	1.682	1.674	1.677	1.683		*1.656*	*1.672*
β	1.700	1.697	1.675	1.691		1.692	1.690	1.689	1.682	1.684	1.689		*1.660*	*1.678*
γ	1.705	1.701	1.680	1.694		1.695	1.691	1.692	1.685	1.687	1.693		*1.669*	*1.682*
$2V_\alpha$ (°)	87.8(2)	77.1(3)	80.4(1)	69.6(3)	64.5(6)	75.7(2)	67.7(2)	60.7(4)	73.2(4)	67.8(3)	77.4(3)			

Table II, continued

Specimen	1	5	6	7	8	11	12	15	17	19	(35)	(1)	(3)
ρ_{obs} (g/cc)	3.393(10)	3.403(10)	3.249(6)	3.314(7)	3.300(6)	3.328(10)	3.281(1)	3.318(3)	3.253(6)	3.275(4)	3.290(5)	3.178	3.289
ρ_{calc} (g/cc)	3.426	3.387	3.255	3.308	3.313	3.357	3.325	3.312	3.278	3.300	3.309	3.202	
$\langle r \rangle$***	0.764	0.759	0.768	0.771	0.778	0.777	0.771	0.775	0.767	0.770			
a (Å)	7.158(6)	7.153(5)	7.156(2)	7.156(2)	7.162(4)	7.161(4)	7.157(1)	7.160(2)	7.153(1)	7.159(2)	7.157(2)	8.933	8.953
b (Å)	9.184(11)	9.169(8)	9.193(3)	9.203(2)	9.208(6)	9.213(6)	9.201(2)	9.209(3)	9.191(2)	9.195(4)	9.200(2)	9.155	9.197
c (Å)	8.958(5)	8.945(7)	8.955(4)	8.960(2)	8.972(6)	8.974(6)	8.962(2)	8.965(3)	8.957(2)	8.958(3)	8.959(2)	7.121	7.145
α (°)	91.97(10)	91.86(6)	91.85(3)	91.83(3)	91.87(4)	91.80(6)	91.85(2)	91.85(3)	91.83(2)	91.83(3)	91.8(3)	102.59	103.03
β (°)	98.31(12)	98.40(6)	98.08(3)	98.08(2)	98.09(7)	98.11(5)	98.15(2)	98.07(3)	98.12(2)	98.09(3)	98.14(2)	98.28	98.10
γ (°)	77.29(8)	77.16(7)	77.35(3)	77.29(2)	77.29(6)	77.24(5)	77.31(1)	77.30(2)	77.33(2)	77.29(3)	77.30(2)	88.09	88.21
Vol (Å^3)	568.5(7)	565.8(5)	569.1(3)	570.0(2)	571.4(4)	571.7(4)	569.9(2)	571.0(2)	568.8(1)	569.5(3)	569.8(2)	568.4	568.2

---

n.d. = not detected. (35) Lattice parameters from Takeuchi et al. (1974). (1) and (3) are from Jobbins et al. (1975)

*B_2O_3 contents were interpolated from curves prepared for pure end-members, H_2O was calculated using the computer program SUPER RECAL of J. C. Rucklidge (personal communication).

**$Tfl = \frac{\text{wt. \% (MnO + FeO + ZnO)}}{\text{wt. \% (MnO + FeO + ZnO + CaO+MgO)}}$

*** $\langle r \rangle$ = mean radius of octahedral cations

Table III

Microprobe analyses, $2V\alpha$, and density measurements for 25 axinites.

Specimen	2	3	4	9	10	13	14	16	18	20	21	22	23
CaO (wt.%)	19.65	19.49	19.76	19.70	19.64	19.94	19.88	19.88	19.62	20.01	20.01	19.70	19.87
MnO	5.66	3.42	2.05	3.35	1.56	2.82	2.17	3.98	4.84	1.32	0.98	2.52	4.87
FeO	4.93	9.32	8.52	6.36	8.52	7.67	8.40	6.70	6.57	8.03	7.53	9.58	6.03
MgO	1.49	0.63	1.49	1.89	1.85	1.44	1.43	1.34	0.79	2.07	2.55	0.73	1.31
ZnO	n.d.	n.d.	n.d.	n.d.	n.d.	n.d.	n.d.	n.d.	n.d.	n.d.	n.d.	n.d.	n.d.
Al_2O_3	17.91	17.14	17.84	18.35	18.34	17.94	18.08	18.01	17.91	18.23	18.23	17.56	17.69
$(B_2O_3)^*$	(6.18)	(6.12)	(6.16)	(6.20)	(6.19)	(6.17)	(6.17)	(6.17)	(6.14)	(6.21)	(6.22)	(6.13)	(6.17)
SiO_2	42.22	41.59	41.88	42.54	42.42	42.03	42.45	42.61	42.25	42.52	42.74	41.83	42.12
$(H_2O)^*$	(1.59)	(1.56)	(1.58)	(1.60)	(1.60)	(1.59)	(1.60)	(1.60)	(1.58)	(1.60)	(1.61)	(1.57)	(1.58)
Sum	99.63	99.27	99.28	99.99	100.12	99.60	100.18	100.29	99.70	99.99	99.87	99.62	99.64
TM**	0.334	0.388	0.332	0.310	0.319	0.329	0.332	0.335	0.359	0.297	0.274	0.372	0.340
$2V_\alpha$ (°)	74.2(7)	68.7(3)	72.0(3)	73.1(1)	73.1(2)	71.4(3)	70.5(5)	72.7(4)	67.8(3)		74.0(1)	67.8(2)	70.5(4)
ρ_{obs} (g/cc)	3.295(7)	3.315(8)	3.292(9)	3.269(5)	3.276(6)	3.295(7)	3.287(5)	3.274(5)	3.290(5)	3.273(6)	3.231(8)	3.298(9)	3.278(6)

n.d. = not detected; *, ** see footnotes in Table 2.

Table III, continued

Specimen	24	25	26	27	28	29	30	31	32	34	36	37
CaO	19.80	19.05	19.12	19.94	19.77	19.78	19.38	18.00	19.25	19.81	18.30	19.76
MnO	3.83	12.33	9.23	3.98	6.20	2.40	5.67	12.74	11.79	1.09	11.79	2.28
FeO	7.95	1.21	3.06	8.41	3.68	7.50	5.99	0.99	0.73	8.76	1.18	8.33
MgO	0.69	0.21	0.49	0.30	1.69	1.73	0.98	0.14	0.14	1.87	0.13	1.53
ZnO	n.d.	n.d.	n.d.	n.d.	n.d.	n.d.	n.d.	2.23	1.80	n.d.	2.20	n.d.
Al_2O_3	18.01	17.47	18.11	17.56	18.23	18.02	17.96	17.30	17.67	17.89	17.38	17.78
$(B_2O_3)^*$	(6.14)	(6.12)	(6.13)	(6.12)	(6.19)	(6.17)	(6.15)	(6.11)	(6.12)	(6.18)	(6.10)	(6.17)
SiO_2	42.44	42.06	41.80	41.98	42.17	41.82	41.84	41.60	42.06	42.12	41.55	42.09
$(H_2O)^*$	(1.59)	(1.58)	(1.58)	(1.58)	(1.59)	(1.58)	(1.58)	(1.58)	(1.57)	(1.59)	(1.57)	(1.58)
Sum	100.45	100.03	99.52	99.87	99.52	99.00	99.55	100.68	101.12	99.31	100.20	99.52
TH	0.365	0.413	0.385	0.380	0.315	0.315	0.362	0.468	0.425	0.312	0.451	0.333
$2V_\alpha$ (°)	67.3(1)	72.5(1)			74.5(4)		71.6(4)	74.1(4)			74.6(4)	
ρ_{obs} (g/cc)						3.272(3)	3.290(3)					

DISCUSSION OF RESULTS

Chemistry

The range in composition of axinites is represented by substitutional solid solution among the divalent, octahedrally-coordinated cations, Ca, Mn, Fe, Mg, and Zn, which can best be seen on two triangular diagrams. Figure 2 has vertices 3Ca - 3Mn - 3(Fe+Mg+Zn). It includes all known axinite compositions (see Tables 2 and 3) and substantiates the conclusions of Sanero and Gottardi (1968) that the major substitutions fall on either of two lines:

$$2Ca \cdot 1(Fe+Mg) \leftrightarrow 2Ca \cdot 1Mn$$

or $$2Ca \cdot 1Mn \leftrightarrow 1Ca \cdot 2Mn.$$

The substitution of Mn for Ca in the distorted Ca1 and Ca2 sites (Fig. 1b) is represented by the numbered specimens in Figure 2: 1, 5, *11*, 25, *31*, *32*, 33, and *36* (those in italics contain zinc). The remainder of the analyses, shown as unnumbered points, plot near the line where Ca ≈ 2.00 atoms per formula unit, and they can best be described separately on a triangular diagram with vertices Mn - Fe - Mg (Fig. 3). This diagram illustrates substitutional relationships in the Fe site (Fig. 1b) and also shows the variation of the optic axial angle $2V_\alpha$ with composition for the 2Ca-axinites.

Silicon was found to be stoichiometric (4.00 atoms per formula unit) within ±1% of the amount present for 36 of 37 analyses. The exception is specimen 7 from Obira, Japan in which a deficiency of 0.089 atoms per formula unit is almost exactly balanced by an excess of 0.090 Al atoms, suggesting a substitution of Al for Si in

Figure 2

A triangular diagram similar to that devised by Sanero and Gottardi (1968) to display the compositional range of the axinites. The unnumbered specimens are also plotted in Figure 3 on an Mn-Fe-Mg diagram. The numbered specimens contain less than 2 Ca atoms.

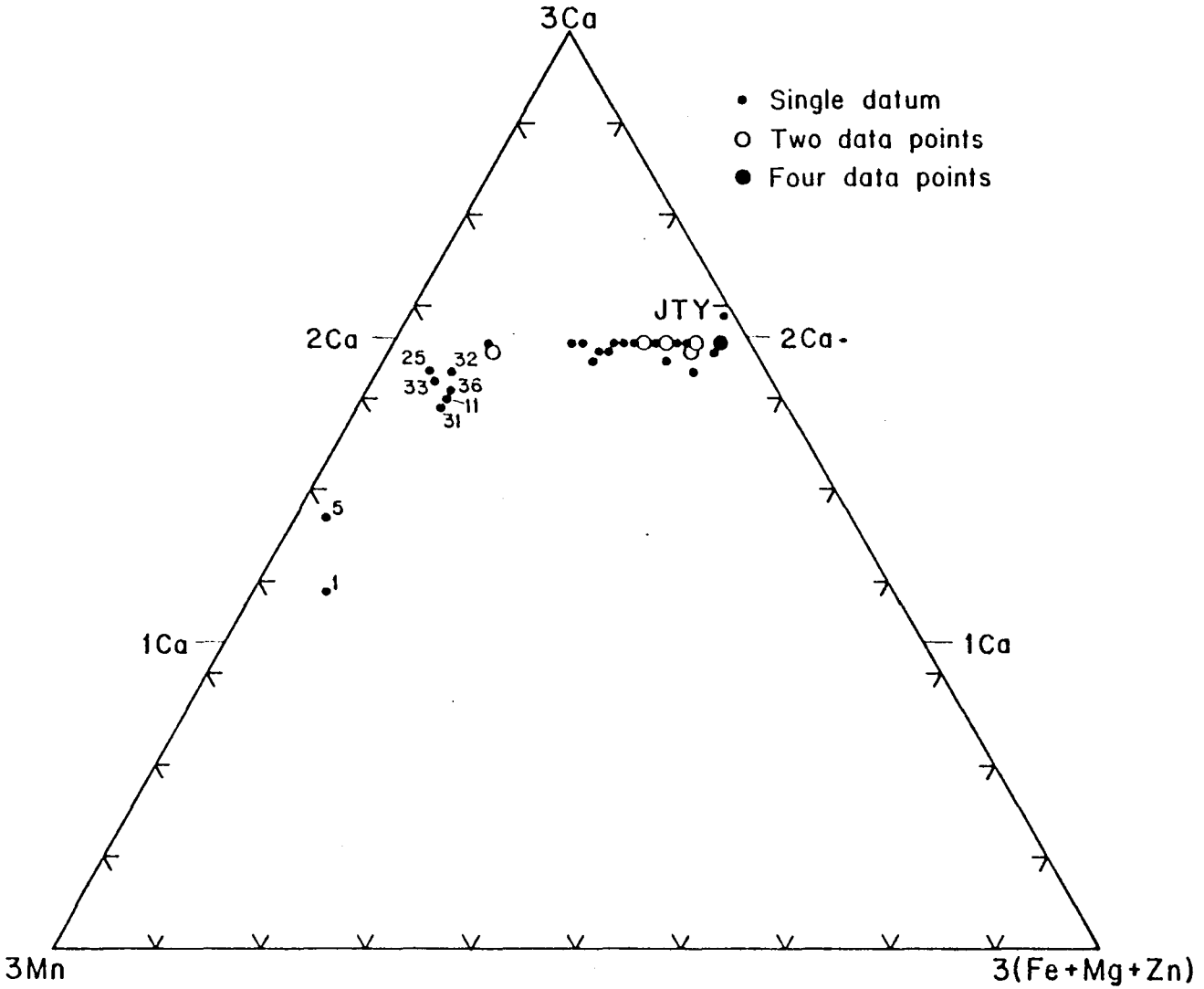
3Ca
• Single datum
o Two data points
● Four data points
JTY
2Ca
2Ca
25
32
33
36
11
31
5
1
1Ca
1Ca
3Mn
3(Fe+Mg+Zn)

Figure 3

A triangular diagram showing the Mn-Fe-Mg contents (normalized to (Mn + Fe + Mg) = 1.00) of 2Ca-axinites. The magnesioaxinite of Jobbins *et al.* (1975) is included on the plot and its 2Vα value, calculated from refractive indices, is shown. This diagram has been partially contoured for 2Vα using data from Tables 2 and 3.

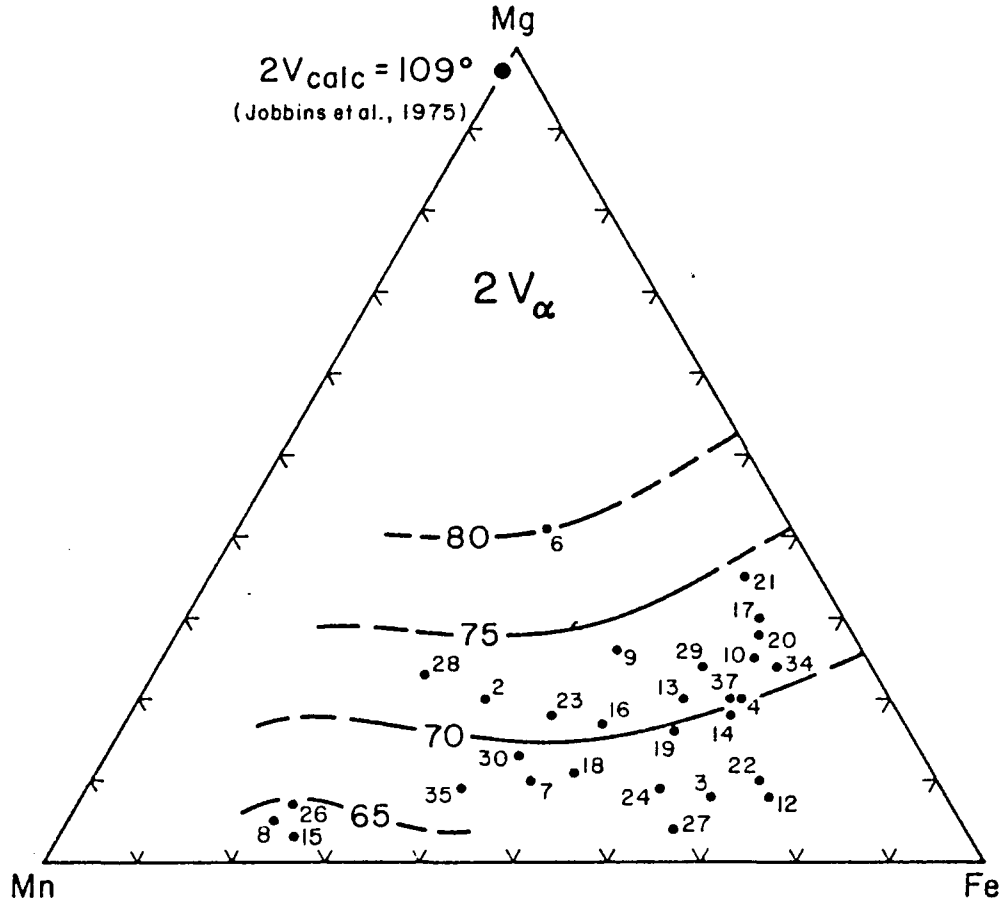
Mg
2Vcalc = 109°
(Jobbins et al., 1975)
2Vα
80
75
70
65
6
21
17
20
9
29
10
34
28
2
13
37
23
16
4
14
19
30
18
22
35
7
24
3
12
26
8
15
27
Mn
Fe

tetrahedral coordination (*cf.* Chaudry and Howie (1969) who suggest a similar substitution in axinites from Devonshire, England).

Except for specimen 7 with 4.5% excess aluminum, presumably in tetrahedral coordination, aluminum was found to be stoichiometric (2.00 atoms per formula unit) within ±2% of the amount present for 30 of the 37 analyses. Specimen 1 from Tinzens, Switzerland, contains the least aluminum (1.78 atoms per formula unit) but shows an excess of 1.22 (Mn+Fe+Mg) normally assigned to the single Fe site. It is presumed that all of the iron (0.20 atoms) in this specimen is Fe^{3+} and that it substitutes for Al^{3+} in the Al1 and Al2 octahedral sites (see Fig. 1b). Specimen 11 from Franklin, New Jersey contains 1.88 Al and 1.19 (Mn+Fe+Mg) -- a slight excess of total cations for the three octahedral sites, but sufficient iron as Fe^{3+} to compensate for "missing" Al in the Al1 and Al2 sites. Similar assumptions can be made concerning specimens 3, 8, 12 and 36 which contain between 1.93 and 1.95 Al atoms and sufficient excess (Mn+Fe+Mg) to allow for a partitioning of Fe^{3+} into the Al sites.

Specimens 11, 31, 32 and 36 from the Fe-Mn-Zn deposits of Franklin, New Jersey are the only axinites containing significant amounts of zinc (1.43 - 2.23 wt.%), and they occur in hydrothermal veins and as products of hydrothermal alteration of calcsilicates (Frondel and Baum, 1974). Specimen 31 is closely associated with a manganoan andradite of composition $Ca_{2.36}Mn_{.67}Mg_{.03}Zn_{.06}Fe^{+3}_{1.46}Al_{.41}Ti_{.03}[Si_3O_{12}]$ and refractive index $n_D = 1.83$.

Structural Formula

Based on the structure refinement of Takéuchi *et al.* (1974) and this and previous chemical investigations, a new structural formula is proposed for axinite:

$$[(Mn,Fe^{2+},Mg,Zn)(Ca_{2-x}Mn_x)(Al_{2-y}Fe^{3+}_y)]^{VI}_2(OH)_2[(B_2Si_{8-z}Al_z)^{IV}O_{30}],$$

where $x < 1$, $y << 1$, $z << 1$, and VI and IV represent the coordination numbers of the cations.

Density

Multiple linear regression analysis of a number of compositional variables together with densities measured on 27 axinites led to the selection of the ratio *TM* (for Transition Metals) ≡ wt.% (MnO+FeO+ZnO)/ wt.%(MnO+FeO+ZnO+CaO+MgO) as the variable most highly correlated to the observed density. Data are shown in Figure 5 and the equation is

$$TM = 2.396\rho_{obs} - 7.530.$$

The correlation coefficient $R^2 = 0.916$. The 2Ca-axinites plot with *TM* values of less than 0.40, whereas axinites with *TM* values greater than 0.40 have less than 2Ca atoms per formula unit.

Forms and Cleavage

Figure 4 is a stereographic projection in which the vectors joining the ends of the A11-A12-A12-A11, A11-Ca2-Fe-Ca1, A12-Ca1-Fe-Ca2 and Ca1-A11-Ca2-A12 octahedral chains are plotted. They all lie on a great circle approximately parallel to the $(\bar{1}11)$ plane in axinite and it is presumed that the orientation of the octahedral layer is well-defined by these chains. The tetrahedral ring, near $(\bar{1}21)$ (Takéuchi

Figure 4

A stereographic projection showing the orientation of the biaxial indicatrix (triangles labeled X, Y, Z) relative to the crystallographic directions (a,b,c) for specimen 11. Also plotted are face poles to the major structural features in axinite, notably the octahedral chains labeled with the sequence of sites encountered along them. The octahedral layer (heavy dashed line) includes all four octahedral chains.

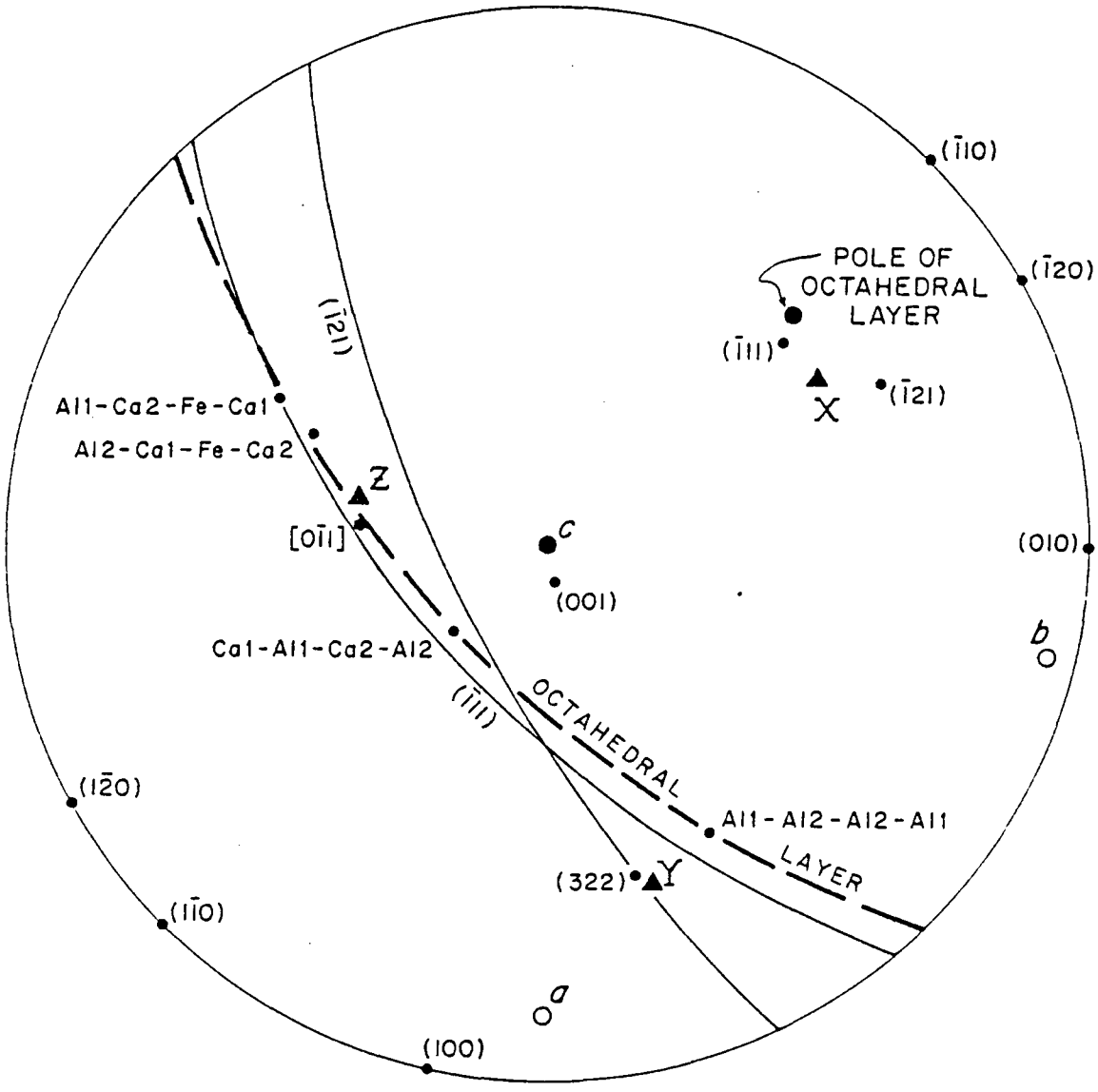
(1̄10)
POLE OF
OCTAHEDRAL
LAYER
(1̄20)
(1̄11)
X
(1̄21)
(1̄21)
Al1-Ca2-Fe-Ca1
Al2-Ca1-Fe-Ca2
Z
[01̄1]
c
(001)
(010)
b
Ca1-Al1-Ca2-Al2
(1̄11)
OCTAHEDRAL
Al1-Al2-Al2-Al1
LAYER
(322)
Y
(12̄0)
(11̄0)
a
(100)

Figure 5

A plot of density versus *TM* for 27 axinites. Calculated densities are indicated by the end of the vertical line extending from the ρ_{obs} data points. JTY refers to the density reported by Jobbins *et al.* (1975) for magnesioaxinite. Specimens with less than 2 Ca atoms per formula unit are circled and numbered.

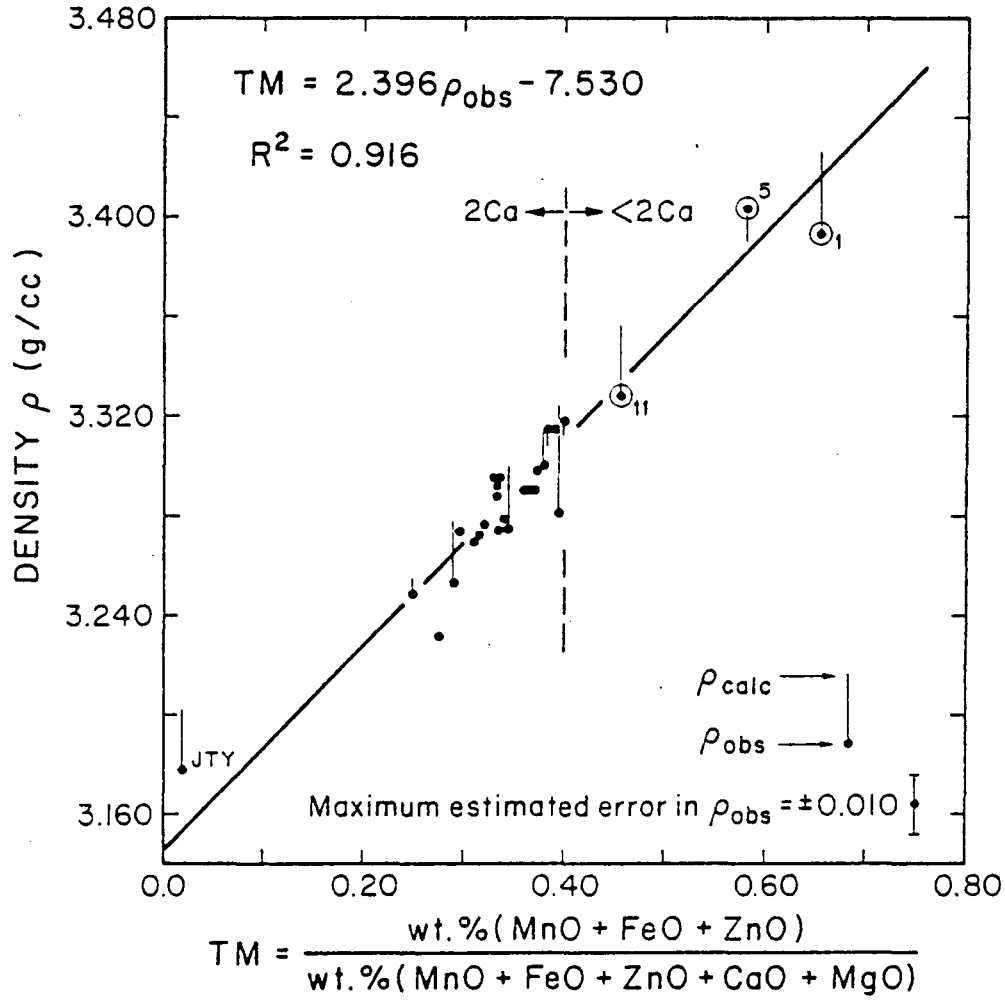
TM = 2.396ρobs - 7.530
R² = 0.916
2Ca
<2Ca
5
1
11
JTY
ρcalc
ρobs
Maximum estimated error in ρobs = ±0.010
DENSITY ρ (g/cc)
3.480
3.400
3.320
3.240
3.160
0.0
0.20
0.40
0.60
0.80
TM = wt.%(MnO + FeO + ZnO) / wt.%(MnO + FeO + ZnO + CaO + MgO)

et al., 1974), is nearly parallel to the octahedral layer. The structural influence of this pronounced layering on external morphology is indicated by a clustering of ($\bar{h}k\ell$) and ($\bar{h}k0$) face poles near the face pole of the octahedral layer (*cf.* Fig. 1 in Peacock, 1937). The planes represented by these face poles generally lie at an angle of 30° or less to the plane of the octahedral layer. Axinite crystals are frequently flattened by some combination of the forms {010}, {011}, {$\bar{1}$11}, {$\bar{1}$21}, {$\bar{1}$10}, and {$\bar{1}$20}.

The {100} cleavage in axinite results from a distinct banding of the $B_2Si_8O_{30}$ groups parallel to [0$\bar{1}$1] in the tetrahedral layer. The dashed lines in Figure 1a show the trace of the {100} cleavage parallel to the elongated $B_2Si_8O_{30}$ group. The cleavage plane is inclined at ∿14° to the plane of the figure. The trace of {100} in the octahedral layer is seen in Figure 1b. Notice that it runs through the hydroxyl groups bonded to Ca2 and both Al1 and Al2. Thus by cleaving on {100}, the integrity of the tetrahedral bands are preserved and only weak (Ca,Al)-(OH,O) and (Fe,Mn,Mg)-O bonds need be broken in the octahedral layer.

Optical Properties

The variation of mean refractive index was also shown by multiple linear regression analysis to be best described in terms of the variable *TM*, and the following equation relating composition to mean refractive index <R.I.> was determined for the data plotted in Figure 6:

$$TM = 15.475\langle R.I.\rangle - 25.700 \qquad (R^2 = 0.965)$$

Figure 6

A plot of mean refractive index versus *TM*. The regression equation refers to the solid line for all data points. The filled circles and dashed line are for axinites with less than 2.0 Ca atoms and the open circles and dotted line are for 2 Ca - axinites (refer to text for regression equations).

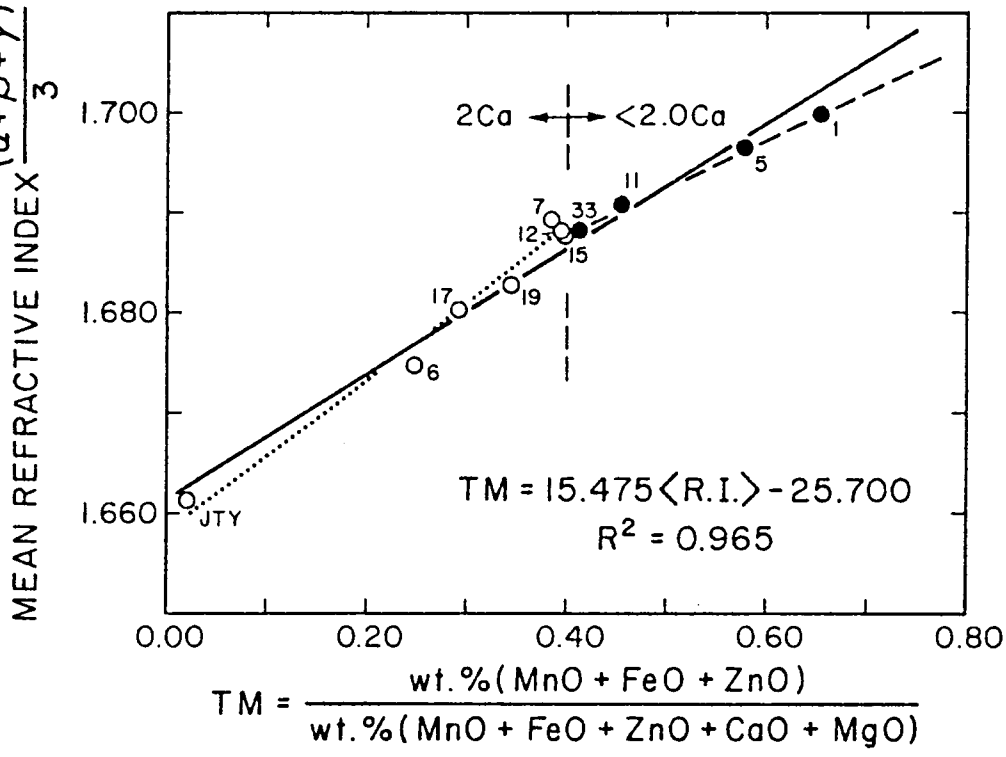
MEAN REFRACTIVE INDEX $\frac{(\alpha+\beta+\gamma)}{3}$
1.700
1.680
1.660
2Ca
<2.0Ca
1
5
11
7
33
12
15
17
19
6
JTY
TM = 15.475⟨R.I.⟩ - 25.700
R^2 = 0.965
0.00
0.20
0.40
0.60
0.80
$TM = \frac{wt.\%(MnO + FeO + ZnO)}{wt.\%(MnO + FeO + ZnO + CaO + MgO)}$

A dashed vertical line at *TM* = 0.40 again serves as a boundary between the 2Ca-axinites and axinites with less than 2Ca atoms per formula unit. Since all of the data points fall within two standard deviations of the line defined by this equation, a second order curve was not fitted to the data; however, it may be possible to describe the variation in mean refractive index with composition by two line segments, one for the 2Ca-axinites defined by the equation:

$$TM = 13.323\langle R.I.\rangle - 22.093 \qquad (R^2 = 0.975)$$

and one for axinites with less than 2Ca atoms per formula unit defined by the equation:

$$TM = 21.443\langle R.I.\rangle - 35.784 \qquad (R^2 = 0.999).$$

As mentioned earlier, Figure 3 was partially contoured to show the variation of the optic axial angle with composition for the zinc-free 2Ca-axinites. It indicates an increase in 2Vα with increasing Mg content. This is probably the result of Mg entering the Fe sites which are located on the ends of the A11-A12-A12-A11 octahedral chains (Fig. 1b) and oriented nearly parallel to Y, the principle vibration direction for the β refractive index (Fig. 4). As Mg substitution increases, n_β decreases at a faster rate than n_α and n_γ, causing an increase in 2Vα and eventually a change in optic sign from negative to positive as shown by the magnesioaxinite of Jobbins *et al.* (1975). The 2Vα value calculated from refractive indices for this nearly pure magnesian end-member is 109.1°.

The orientation of the biaxial indicatrix in relation to the crystallographic directions and structural features of axinite is

presented in Figure 4 for specimen 11. The Z principle vibration direction is oriented nearly parallel to [0$\bar{1}$1] which is the direction of elongation of the $B_2Si_8O_{30}$ groups (*cf.* Fig. 1a), and plots between the poles representing the directions of the three Ca-containing octahedral chains. As mentioned earlier, Y is oriented near the All-Al2-Al2-All octahedral chains which are terminated at each end with Fe-octahedra (*cf.* Fig. 1b), and X is at an angle of ∿79° to the octahedral layer and ∿80° to the ($\bar{1}$21) plane of the tetrahedral $B_2S_4O_{12}$ ring. This indicatrix orientation is similar to that found in the optically negative micas where Z and Y lie parallel or nearly parallel to the plane of the tetrahedral and octahedral layers and X is normal or nearly normal to the plane of layering.

Lattice Parameters

The lattice parameters of each of 10 axinites were determined using 30 to 40 powder diffraction peaks in the range 9 - 70°2θ; they are recorded in Table 2. The cell edges *a*, *b* and *c* are plotted in Figure 7 as a function of <r>, the mean radius of cations occupying the Cal, Ca2, Fe, All and Al2 octahedral sites. Their variation can best be discussed with reference to the stereonet in Figure 4. Unfortunately the reduced triclinic cell of axinite leaves none of the axial zones oriented along major structural features. The zone [0$\bar{1}$1] comes closest to the octahedral chains All-Ca2-Fe-Cal, Al2-Cal-Fe-Ca2 and Cal-All-Ca2-Al2, among which the primary cation substitutions occur. Thus it is not surprizing that the linear regression equations for *b* (inclined at 32° to chain All--- and at 36° to chain Al2---), for *c*

Figure 7

The lattice parameters a, b, and c of the axinites listed in Table 2, plotted versus <r>, the mean radius of cations occupying the Ca1, Ca2, Fe, Al1 and Al2 octahedral sites. Error bars are shown for each datum, and the cell edges of Takéuchi *et al.* (1974), which were not used in the regression, are included for comparison (open circles). The lattice parameters determined by Jobbins *et al.* (1975) and listed in Table 2 fall significantly below these curves; they were not plotted because the authors gave no indication of the use of an internal standard.

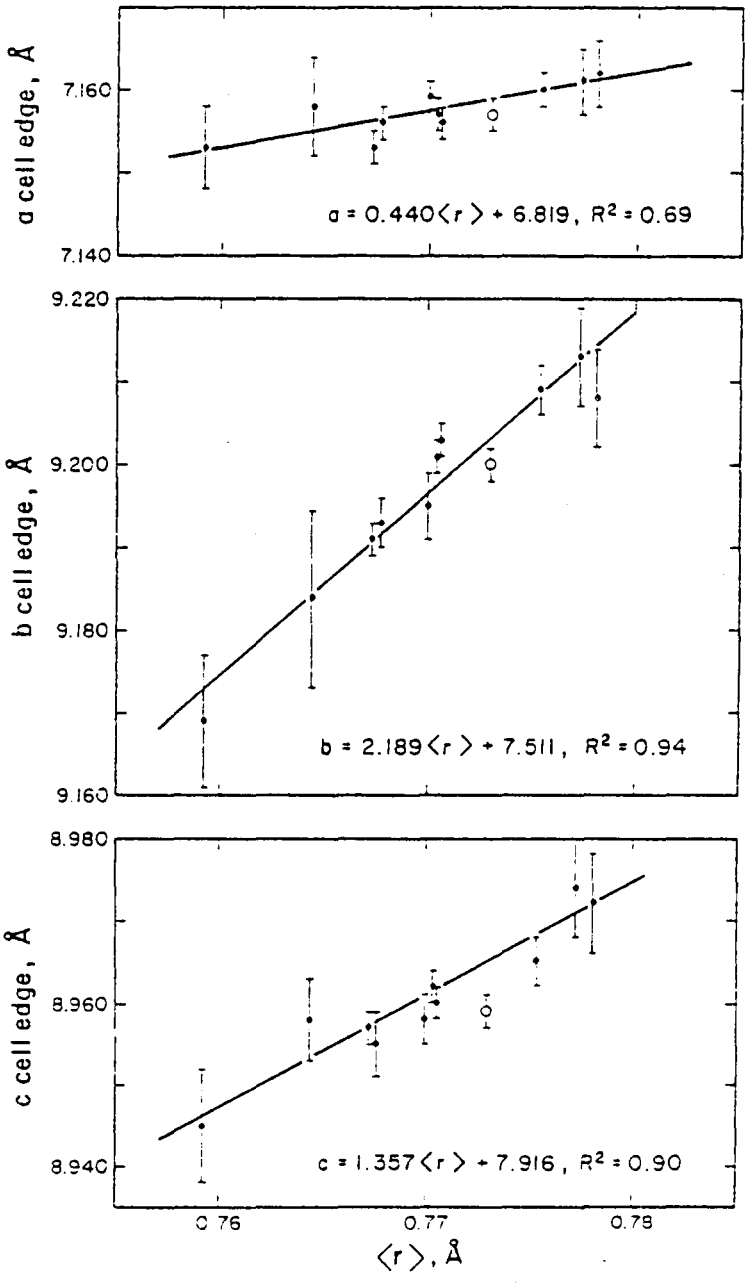
a cell edge, Å
7.160
7.140
a = 0.440⟨r⟩ + 6.819, R² = 0.69
b cell edge, Å
9.220
9.200
9.180
9.160
b = 2.189⟨r⟩ + 7.511, R² = 0.94
c cell edge, Å
8.980
8.960
8.940
c = 1.357⟨r⟩ + 7.916, R² = 0.90
0.76
0.77
0.78
⟨r⟩, Å

(inclined at 50 and 58° to All--- and Al2--- and at 26° to chain Cal---) and for a (inclined at high angles to all these octahedral chains) have slopes in the ratio 5:3:1 and coefficients of correlation R^2 = 0.94, 0.90 and 0.69. As anticipated, the unit cell volume is most highly correlated with $\langle r \rangle^3$ (see Fig. 8).

Composition of 2Ca-axinites from Optical Properties and Density

Mean refractive index, 2Vα, and density for 7 non-zincian 2Ca-axinites were used to determine multiple linear regression equations for the individual calculations of the mole fractions of Mg, Fe, and Mn using the Biomedical Computer Program BMD03R (Dixon, 1973). The results are tabulated below; standard errors of regression coefficients are listed in parentheses below the coefficient.

$$\underset{}{Mg} = \underset{(3.268)}{-14.333\langle R.I.\rangle} + \underset{(0.002)}{0.012(2V\alpha)} + 23.487 \qquad (R^2 = 0.997)$$

$$Fe = \underset{(14.547)}{71.937\langle R.I.\rangle} - \underset{(3.042)}{11.810(\rho_{obs})} - 81.890 \qquad (R^2 = 0.894)$$

$$Mn = \underset{(12.445)}{-42.903\langle R.I.\rangle} + \underset{(2.602)}{12.523(\rho_{obs})} + 31.473 \qquad (R^2 = 0.910)$$

The pair of variables in each equation above is the combination having the greatest statistical significance. Inclusion of ρ_{obs} in the equation for Mg resulted in a decrease in the F-ratio from 577 to 311 and a $|t|$ value for ρ_{obs} of 0.197 which may be rejected at the 20% confidence level. Inclusion of 2Vα in the equations for Fe and Mn results in decreased F-ratios and $|t|$ values of 0.960 and 0.380 respectively which can be rejected as being significant at the 60% and 30% confidence levels, respectively. A plot of calculated versus observed Mg, Fe, and Mn mole fractions (Fig. 9) suggests that the

Figure 8

A plot of the unit cell volume of axinite versus the cube of the mean radius of cations occupying the Ca1, Ca2, Fe, Al1 and Al2 sites. The datum of Takéuchi *et al.* (1974) is plotted as an open circle for purposes of comparison.

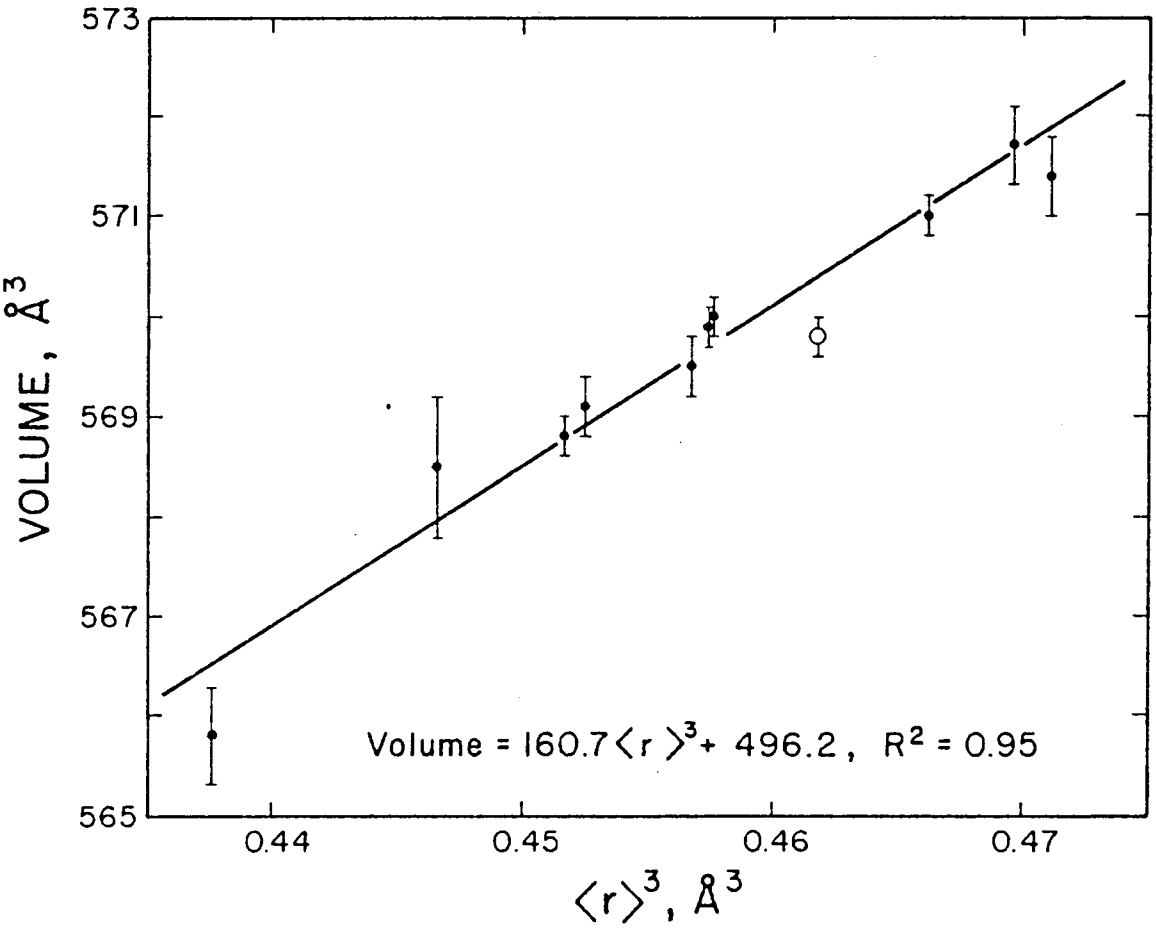
573
571
569
567
565
VOLUME, Å3
0.44
0.45
0.46
0.47
⟨r⟩3, Å3
Volume = 160.7⟨r⟩3 + 496.2, R2 = 0.95

Figure 9

A combined plot of the observed mole fractions of Mg, Fe, and Mn for seven axinites versus the values calculated from the multiple regression equations given in the text. Both observed and calculated values were normalized to (Mg+Fe+Mn) = 1.00 before plotting, because totals ranged between 0.95 and 1.05. The line has a slope of 45°.

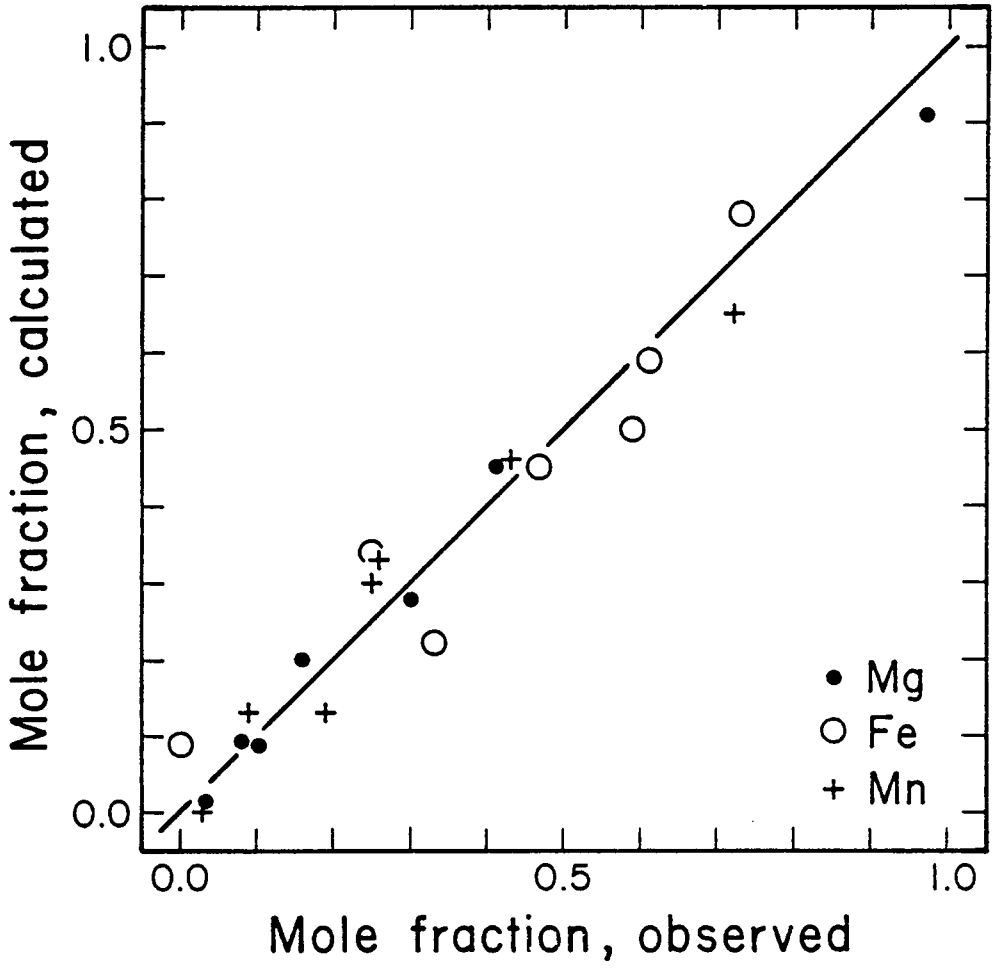
1.0
0.5
0.0
0.0
0.5
1.0
Mole fraction, calculated
Mole fraction, observed
Mg
Fe
Mn

above equations provide a reasonable estimate of composition for the non-zincian 2Ca-axinites. However, better correlations based on identical variables should result for the three equations upon acquisition of additional data for multiple regression analysis.

The $2V\alpha$ values for the numbered specimens in figure 2 do not at all fit the pattern of the non-zincian 2Ca-axinites (unnumbered in Fig. 2) plotted in Figure 3. The zinc-bearing Franklin, New Jersey specimens (11, 31 36) have 2V values of 75.7°, 74.1° and 74.6°, respectively. Specimens 25 and 33 with nearly the same composition (Tables 2 and 3) have $2V\alpha$ =72.5° and 77.4°, and specimen 5 with 1.42 Ca and specimen 1 with 1.26 Ca have 2V values of 77.1° and 87.8°, respectively. Clearly there remains a considerable amount of study required to complete the optical characterization of the axinites.

CONCLUSIONS

Based on the results of this work and previous studies, the chemistry of the axinite group can best be expressed by the structural formula

$$[(Mn,Fe^{2+},Mg,Zn)(Ca_{2-x}Mn_x)(Al_{2-y}Fe^{3+}_y)]^{VI}_2(OH)_2[(B_2Si_{8-z}Al_z)^{IV}O_{30}],$$

where $x < 1$, $y << 1$, and $z << 1$. The physical properties of axinite are influenced by the major structural features including the layering approximately parallel to $(\bar{1}11)$, bands of $B_2Si_8O_{30}$ groups parallel to $[0\bar{1}1]$, and four types of finite octahedral chains. Density and mean refractive index are highly correlated with the amount of transition metal oxides present for the known range of axinite compositions and contrary to previous statements, $2V\alpha$ is highly correlated with composition for the non-zincian 2Ca-axinites.

It is evident that much more data is needed to fully characterize the variation of $2V\alpha$ for the axinites with less than 2Ca atoms per formula unit and to refine the equations for estimating the composition of non-zincian 2Ca-axinites. Future research might also be directed toward the petrology and geological occurrences of axinite.

REFERENCES

APPLEMAN, D.E., and H.T. EVANS, Jr. (1973) Job 9214: Indexing and least-squares refinement of powder diffraction data. Natl. Tech. Inf. Serv., U.S. Dept. Commer., Springfield, Virginia, Document *PB 216 188*.

ASTAKHOV, A.V., Yu.B. VOITKOVSKII, O.N. GENERALOV, and S.V. SIDOROV (1976) NGR investigation of some lamellar and boron-containing silicates. *Soviet Phys. Cryst. 20*, 471-474.

BARBOUR, E.A., H.H. BIRD, and D.P. GOLD (1957) An occurrence of axinite in Ventersdorp lavas from Kinross, Transvaal, South Africa. *Mineral. Mag. 31*, 495-496.

BERMAN, H. (1939) A torsion microbalance for the determination of specific gravities of minerals. *Am. Mineral. 24*, 434-440.

BLOSS, F.D. (in press) *The Spindle Stage: Principles and Practice*. Geopress, P.O. Box 662, Blacksburg, VA 24060.

———, and D. RIESS (1973) Computer determination of 2V and indicatrix orientation from extinction data. *Am. Mineral. 58*, 1052-1061.

CHAUDRY, M.N., and R.A. HOWIE (1969) Axinites from the contact skarns of the Meldon Aplite, Devonshire, England. *Mineral. Mag. 37*, 45-48.

DANA, E.S. (1892) *System of Mineralogy*, 6th Ed. p. 529.

DIXON, W.J., ed. (1973) *BMD, Biomedical Computer Programs*. Univ. of Calif. Press, Berkeley, 773 pp.

EREMENKO, G.K. (1971) Optical absorption spectra of axinite group minerals. *Dopov. Akad. Nauk UKR. RSR, Ser. B 33(9)*, 783-788.

FORD, W.E. (1903) On the chemical composition of axinite. *Am. J. Sci. 165*, 195-201.

FRONDEL, C., and J.L. BAUM (1974) Structure and mineralogy of the Franklin zinc-iron-manganese deposit, New Jersey. *Econ. Geol. 69*, 157-181.

GÄDEKE, R. (1938) Die Gesetzmässigen Zusammenhänge und Anomalien in der Vesuviangruppe und einigen anderen Kalksilikaten. *Chem. der Erde (Linck) 11*, 592-636.

GENTH, F.A. (1891) Contributions to mineralogy, no. 50. *Am. J. Sci. 141*, 394-395.

HINTZE, C. (1897) *Handbuch der Mineralogie 2*, 508-509.

ITO, T., and Y. TAKÉUCHI (1952) The crystal structure of axinite. *Acta Crystallogr. 5*, 202-208.

———, ———, T. OZAWA, T. ARAKI, T. ZOLTAI, and J.J. FINNEY (1969) The crystal structure of axinite revised. *Proc. Japan Acad. 45*, 490-494.

JAKOB, J. (1923) Vier Mangansilikate aus den Val D'Err (Kanton, Graubünden). *Schweiz. Mineral. Petrogr. Mitt. 3*, 227-236.

——— (1926) Die Tinzenite-Varietäten aus dem Val D'Err (Graubünden). *Schweiz. Mineral. Petrogr. Mitt. 6*, 200-202.

——— (1933) Die Manganerzlagrstätten zwischen Val D'Err und Rouna (Oberhalbstein), ihre Begleitminerale und ihre Genesis. *Schweiz. Mineral. Petrogr. 13*, 17-39.

JOBBINS, E.A., A.E. TRESHAM, and B.R. YOUNG (1975) Magnesioaxinite, a new mineral found as a blue gemstone from Tanzania. *J. Gemmol. 14*, 368-375.

MILTON, C., F.A. HILDEBRAND, and A.M. SHERWOOD (1953) The identity of tinzenite with manganoan axinite. *Am. Mineral. 38*, 1148-1158.

MOENKE, H. (1962) Fortschritte auf dem Gebiet der Ultrarotspektrosopie II. Nachweis von BO_3- und BO_4-Gruppen in den Haufigsten Naturlich Gebildeten Silikaten. *Silikat. - Techn. 13*, 287-288.

PARKER, R.L. (1948) Zur Kristallographie von Tinzenit. *Schweiz. Mineral. Petrogr. Mitt. 28*, 475-492.

PEACOCK, M.A. (1937) On the crystallography of axinite and the normal setting of triclinic crystals. *Am. Mineral. 22*, 588-624.

PLYUSINA, I.I. (1961) Infrared spectra of ring silicates. III. *Zh. Strukt. Khim. 2*, 330-336.

SANERO, E., and G. GOTTARDI (1968) Nomenclature and crystal chemistry of axinites. *Am. Mineral. 53*, 1407-1411.

SCHALLER, W.T. (1911) Mineralogical notes, Series I, Axinite from California. *U.S.G.S. Bull. 490*.

TAKÉUCHI, Y., T. OZAWA, T. ITO, T. ARAKI, T. ZOLTAI, and J.J. FINNEY (1974) The $B_2Si_8O_{30}$ groups of tetrahedra in axinite and comments on the deformation of Si tetrahedra in silicates. *Zeits. Kristallogr. 140*, 289-312.

WALDMANN, H. (1948) Über die Kristalloptik von Tinzenit. *Schweiz. Mineral. Petrogr. Mitt. 28*, 493-501.

The vita has been removed from the scanned document

CHEMISTRY AND PHYSICAL PROPERTIES OF AXINITES

by

Gregory Randolph Lumpkin

(ABSTRACT)

Electron microprobe analyses of 37 axinites substantiate the conclusions of Sanero and Gottardi (1968) as to the substitutional solid solution between octahedrally coordinated divalent cations Ca, Fe, and Mn. The analyses also suggest the substitution of Fe^{3+} for Al in the $AlO_5(OH)$ octahedra for six axinites and the substitution of Al for Si in tetrahedral coordination for one specimen. The chemistry of the axinite group is best described by a new structural formula:

$$[(Mn,Fe^{2+},Mg,Zn)(Ca_{2-x}Mn_x)(Al_{2-y}Fe^{3+}_y)]^{VI}_2(OH)_2[(B_2Si_{8-z}Al_z)^{IV}O_{30}],$$

where $x < 1$, $y << 1$, and $z << 1$.

Pronounced layering approximately parallel to $(\bar{1}11)$, bands of $B_2Si_8O_{30}$ groups parallel to $[0\bar{1}1]$, and four types of octahedral chains influence indicatrix orientation, external morphology, and cleavage. Due to their proximity to octahedral chains, the b and c cell edges have high correlations with <r>, the mean radius of octahedral cations. Density and mean refractive index are shown to be highly correlated with the amount of transition metal oxides present for all axinites and $2V\alpha$ is highly correlated with Mg content for the non-zincian 2Ca-axinites. Reasonable estimates of composition can be obtained for the non-zincian 2Ca-axinites by using the following equations for the mole fraction of Mg, Fe, and Mn:

$$Mg = -14.333\langle R.I.\rangle + 0.012(2V\alpha) + 23.487$$

$$Fe = 71.937\langle R.I.\rangle - 11.810(\rho_{obs}) - 81.890$$

$$Mn = -42.903\langle R.I.\rangle + 12.523(\rho_{obs}) + 31.473.$$